RSC Advances

PAPER

View Article Online
View Journal | View Issue

Cite this: *RSC Adv.*, 2021, **11**, 13164

Enhanced gas separation and mechanical properties of fluorene-based thermal rearrangement copolymers

Jianhua Zhang,[a] Yunhua Lu,[a] Guoyong Xiao,[a] Mengjie Hou,[b] Lin Li[b] and Tonghua Wang*[b]

A series of thermal rearrangement (TR) copolymer membranes were prepared by the copolymerization of 9,9-bis(3-amino-4-hydroxyphenoxyphenyl) fluorene (BAHPPF), 9,9-bis(3-amino-4-hydroxyphenyl)fluorene (BAHPF) and 2,2′-bis(3,4′-dicarboxyphenyl)hexafluoropropane dianhydride (6FDA), followed by thermal imidization and further thermal rearrangement. The effects of molar ratio of diamines on the structure and properties of copolymer membranes were studied. The copolymer precursors CP-4:6 and CP-5:5 exhibited excellent mechanical properties. The mechanical properties of precursor membranes rapidly decreased with the increase of thermal treatment temperatures, but the tensile strength of TRCP-4:6 still reached 21.2 MPa. In general, the gas permeabilities of TR copolymers increased with the increase of BAHPF content. Comparatively, TRCP-3:7 and TRCP-4:6 showed higher gas permeabilities, coupled with high O_2/N_2 and CO_2/CH_4 selectivities. Especially, the H_2, CO_2, O_2, N_2 and CH_4 permeabilities of TRCP-4:6 reached 244.4, 269.0, 46.8, 5.20 and 4.60 Barrers respectively, and the selectivities for CO_2/CH_4 and O_2/N_2 were 58.48 and 9.00, which exceeded the 2008 upper bound. Therefore, these TR copolymer membranes are expected to be one of the candidate materials for gas separation applications.

Received 23rd December 2020
Accepted 30th March 2021

DOI: 10.1039/d0ra10775a

rsc.li/rsc-advances

1. Introduction

Membrane separation has many advantages, such as simple process, high efficiency, saving energy consumption, low cost and space-efficient, and has exhibited broad application prospects, including hydrogen purification, CO_2 capture in natural gas, gas dehumidification, organic mixed gas separation and recovery.[1–3] At present, the commercial gas separation membranes are mainly polymeric membranes, involving cellulose acetate (CA), polyphenylene ether (PEO), polyimide (PI), *etc.*[4–6] These separation membranes rely on a close packed structure and appropriate chain rigidity to form tiny gas transmission channels, so they usually display high separation selectivities but low gas permeabilities. According to the Robeson's 1991 and 2008 gas separation upper limits, most of the commercial membranes operate under the upper limit, meaning a low work efficiency.[7–9] Therefore, the development of high-performance membrane materials with high gas permeabilities and selectivities is urgently needed.

In recent years, thermal rearrangement (TR) polymers have attracted the attention of researchers due to their excellent gas separation performance.[10–15] TR polymers are mostly based on hydroxy-containing polyimide (HPI) as precursors. After proper thermal treatment, HPI first forms a carboxy–benzoxazole intermediate, and then decarboxylates to generate a heteroaromatic benzoxazole structure.[16–18] In TR polymers, the rotation and movement of benzoxazole ring and phenylene group are relatively difficult, which enhances the rigidity of polymer chain and gives the polymers high free volume fraction.[19–22] It is reported that the bimodal microporous structure of TR polymers is in the range of 0.3–0.4 Å and 0.7–0.9 Å.[23–26] The unique hourglass structure allows the TR polymer to have both high gas permeabilities and selectivities simultaneously.[27–30] However, the trade-off relationship between gas permeabilities and selectivities still exists, so for some gas pairs, such as O_2/N_2 and CO_2/CH_4, the separation performance of TR polymers needs to be further improved to meet the practical applications. Therefore, many HPI precursors with novel chemical structures have been designed to improve the separation performance of membrane materials.[31–36]

As we have known that the rigid and bulky structures easily destroy the regular arrangement of molecular chains, reduce the interaction between molecular chains, and increase the free volume fraction, leading to high gas permeabilities and moderate selectivities.[37–42] For example, Fahd *et al.* introduced the triptycene structures into the main chain of TR polymer, so the permeability of O_2 was 311 Barrer, and the O_2/N_2 selectivity was 5.4, which was close to the 2008 upper bound.[43] In addition, the rigid and large volume fluorene groups are helpful to hinder

[a]School of Chemical Engineering, University of Science and Technology Liaoning, Anshan, Liaoning, 114051, P. R. China. E-mail: lee.lyh@163.com; Fax: +86 412 5216702; Tel: +86 412 5929952

[b]School of Chemical Engineering, Dalian University of Technology, Dalian, Liaoning 116024, P. R. China. E-mail: wangth@dlut.edu.cn

the entanglement and rotation of molecular chain, and increase the spacing between the molecular chains, resulting in high permeabilities of TR membranes.[44–46] Generally, TR polymers derived from rigid macromolecular chains exhibit excellent gas separation properties, but they often require higher rearrangement temperatures and show poor mechanical properties. On the contrary, TR polymers based on flexible chain skeletons show lower rearranged temperatures and higher gas selectivities, but the gas permeabilities are relatively weakened to some extent.[45,46] Hence, adjusting the rigidity of macromolecular chain by copolymerization is an effective way to obtain TR membranes with excellent comprehensive properties.

Our research group found that the TR polymers derived from 9,9-bis(3-amino-4-hydroxyphenyl)fluorene (BAHPF) displayed poor mechanical properties, film-formation and high thermal rearrangement temperatures, while the TR polymers based on 9,9-bis[4-(4-amino-2-hydroxyphenoxy)phenyl]fluorene (BAHPPF) exhibited good film-formation and mechanical properties, but low gas permeabilities.[45,46] It is expected that the TR membranes exhibit excellent separation performance and moderate mechanical properties to meet the practical applications. Therefore, in this study, a series of TR copolymer membranes were prepared by the copolymerization of BAHPF, BAHPPF and 2,2′-bis(3,4′-dicarboxyphenyl)hexafluoropropane dianhydride (6FDA), followed by thermal imidization and further rearrangement. The effects of molar ratio of diamines on the structure, mechanical, thermal properties and gas separation performance of copolymer membranes were investigated by FTIR, XRD, XPS, DSC, DMA, tensile testing and gas permeabilities measurement. The final gas separation properties were easily adjusted by copolymerization ratio, and the mechanical properties of the TR membranes were also kept as much as possible. Thus, the fluorene-containing TR copolymer membranes will be potential candidate materials in the field of gas separation application.

2. Experimental

2.1 Materials

9,9-Bis(3-amino-4-hydroxyphenyl)fluorene (BAHPF) and 9,9-bis[4-(4-amino-2-hydroxyphenoxy)phenyl]fluorene (BAHPPF) were synthesized according to our reported method.[45,46] 2,2′-bis(3,4′-dicarboxyphenyl)hexafluoropropane dianhydride (6FDA) was obtained from Chinatech (Tianjin) Chemical Co., Ltd, dried at

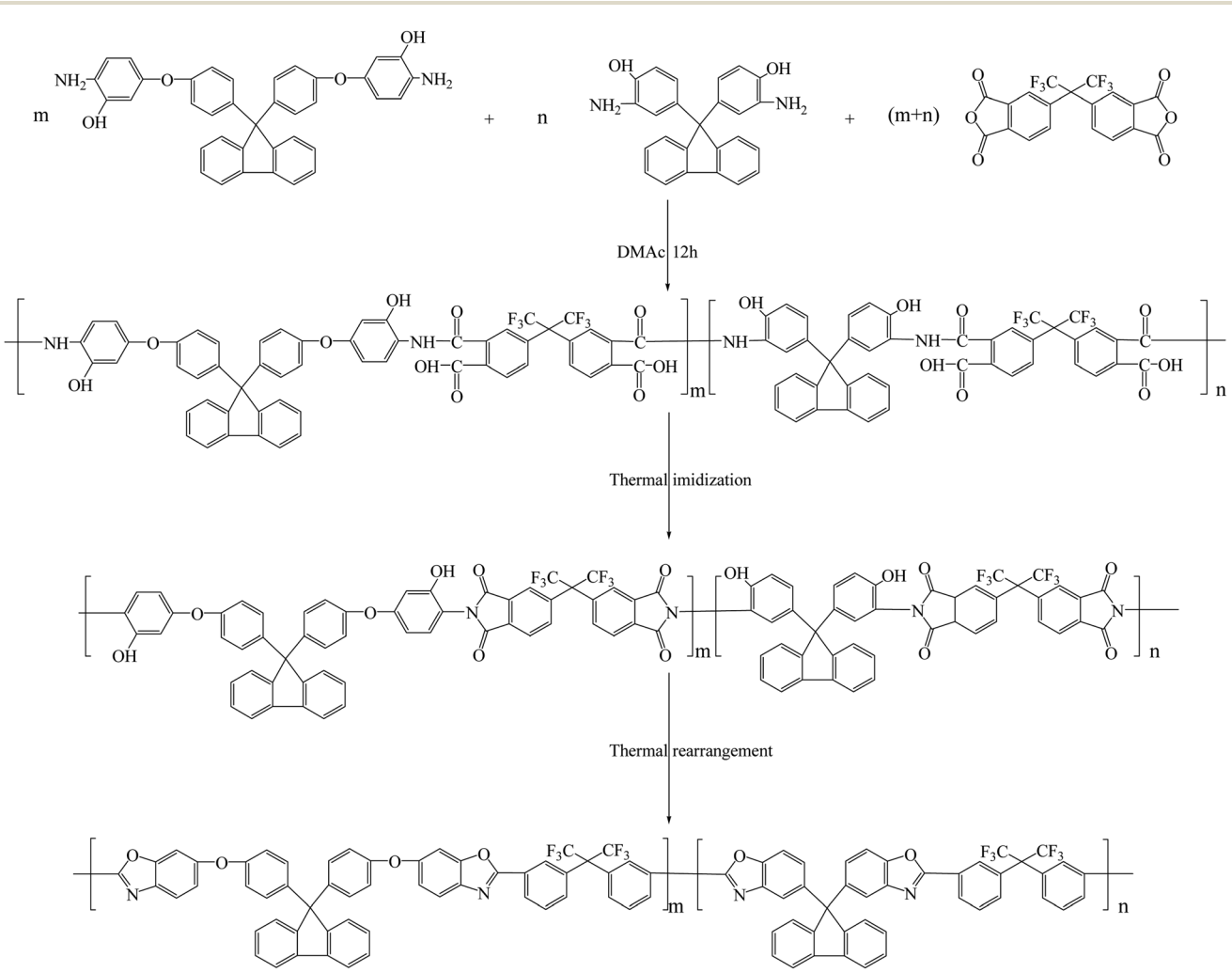

Scheme 1 Synthesis of thermally rearranged copolymers.

180 °C for 24 hours in a vacuum oven before use. *N*,*N*-Dimethylacetamide (DMAc) was purchased from Sinopharm Chemical Reagent Co., Ltd (China) without any treatment.

2.2 Preparation of copolymer precursors

Firstly, BAHPF and BAHPPF were copolymerized with 6FDA in varying molar ratios to form the poly(amic acid) (PAA) solution, followed by thermal imidization to obtain copolymer precursors, as shown in Scheme 1. Taking the synthesis of CP-5:5 as an example: BAHPF (0.005 mol, 1.9023 g), BAHPPF (0.005 mol, 2.8232 g) and DMAc (55.3 mL) were added to a two-neck 250 mL flask equipped with a mechanical stirrer in ice water bath. After the diamines were completely dissolved, 6FDA (0.01 mol, 4.4424 g) was introduced and continuously stirred for 12 hours to form a homogeneous PAA solution with a concentration of 15 wt%. Then, the PAA solution was evenly spread on a clean glass plate with a glass rod, and kept on a constant temperature platform at 40 °C for 24 hours to slowly evaporate the most solvent. In a far-infrared oven, the sample was further heated at 80 °C for 1 hour, 150 °C for 1 hour and 250 °C for 0.5 hour. After natural cooling, the sample was immersed in hot water at 60 °C for at least 30 minutes to remove the membrane from the glass plate, and the obtained membrane was further dried in a vacuum oven at 100 °C for 24 hours. The copolymer precursor (CP) was called as CP-5:5. According to the same procedure, other copolymer membranes CP-9:1, CP-8:2, CP-7:3, CP-6:4, CP-4:6, CP-3:7 and CP-2:8, were also prepared. Here, the ratio of two numbers represents the molar ratio of BAHPPF to BAHPF.

2.3 Preparation of TR copolymer membranes

The above membranes were cut into 2 cm × 2 cm square samples and sandwiched between two graphite plates. Then, the samples were placed into a tube furnace and heated to 450 °C at a heating rate of 3 °C min^{-1} and kept for 1 hour in nitrogen atmosphere (200 mL min^{-1}). Finally, the furnace was naturally cooled down to room temperature. Here, the obtained membranes were named as TRCP-9:1, TRCP-8:2, TRCP-7:3, TRCP-6:4, TRCP-5:5, TRCP-4:6, TRCP-3:7 and TRCP-2:8, respectively.

2.4 Characterization

The mechanical properties of copolymer membranes were tested by HY0350 tensile testing machine (Shanghai Hengyi Precision Instrument Co., Ltd, China) with a tensile rate of 10 mm min^{-1}. The sample size was 8 cm × 1 cm, and the gauge distance was 5 cm. At least three samples were cut from each membrane, and the average value of mechanical properties was calculated. The dynamic mechanical properties of copolymer samples were studied by Dynamic thermomechanical analyzer DMA 8000 (PerkinElmer, USA) from 50 to 400 °C at a heating rate of 10 °C min^{-1} with 1 Hz in N_2 atmosphere (80 mL min^{-1}). Glass transition temperatures (T_g) of TR samples were measured by a PerkinElmer Instruments DSC 4000 from 50 to 400 °C with a heating rate of 20 °C min^{-1} in nitrogen atmosphere (19.8 mL min^{-1}). The second scanning curves were used to estimate the T_g value. The weight losses of copolymer samples were recorded by Pyris 1 TGA thermogravimetric analyzer (PerkinElmer, UAS) at a heating rate of 10 °C min^{-1} and a nitrogen purge of 50 mL min^{-1} in the range of 50–700 °C.

The Fourier transform infrared (FTIR) measurements were conducted on a Nicolet IS 10 spectrometer (USA) from 4000 to 500 cm^{-1}. Wide-angle X-ray diffraction (WAXD) was performed on X′ Pert Powder X-ray diffractometer (PANalytical, Almelo, Netherlands) from 5° to 70° with copper K_α radiation (operating at 40 kV and 40 mA) to show the changes in intersegmental properties of these samples. The average *d*-spacing values were calculated according to Bragg's law using eqn (1):

$$n\lambda = 2d \sin \theta \quad (1)$$

where n is an integral which is equal to 1, λ is the wavelength of the Cu source (1.54178 Å), θ represents the diffraction angle and d represents the average spacing between polymer chains. X-ray photoelectron spectroscopy (XPS) spectra was obtained by an ESCALAB 250Xi spectrometer (Thermo Fisher, USA).

The traditional constant pressure-variable volume method was used to characterize the gas permeabilities of the membranes with the high purity gas (>99.99%), including H_2, O_2, N_2, CO_2 and CH_4. The test temperature was 30 °C, and the pressure was 0.01 MPa. The calculation of gas permeability followed eqn (2).

$$P_i = \frac{F/S}{\Delta P/L} \quad (2)$$

P_i is the membrane permeability of i gas, Barrer (1 Barrer = 1×10^{-10} $cm_{(STP)}{}^3$ cm cm^{-2} s^{-1} $cm_{Hg}{}^{-1}$); F is the volume flow of permeated gas, $cm_{(STP)}{}^3$ s^{-1}; S is the effective area of the sample membrane, cm^2; ΔP is the pressure difference between the upstream and downstream of the sample, Pa; L represents for the film thickness, cm. The calculation of gas selectivity is shown in eqn (3), where $\alpha_{1/2}$ is the rational selectivity of gas 1 equivalent to gas 2.

$$\alpha_{1/2} = \frac{P_1}{P_2} \quad (3)$$

3. Results and discussion

3.1 Synthesis and characterization of copolymer precursors

The images of eight kinds of copolymer precursors and CP-4:6 treated at 350, 400 and 450 °C are shown in Fig. 1. These precursor membranes exhibited yellow or brown and transparent, and the color of precursor membranes turned to black after thermal rearrangement at 450 °C for 1 hour. All obtained TR copolymer membranes could be bent to some extent, especially TRCP-4:6 and TRCP-5:5, indicating that these TR copolymers exhibited excellent flexibility.

The infrared spectra of copolymer precursors are shown in Fig. 2. It can be seen that all of curves show the characteristic peaks of the imide ring at 1785 and 1719 cm^{-1}, which corresponds to symmetrical stretching vibration and bending vibration of C=O in the imide group, respectively. The peak at

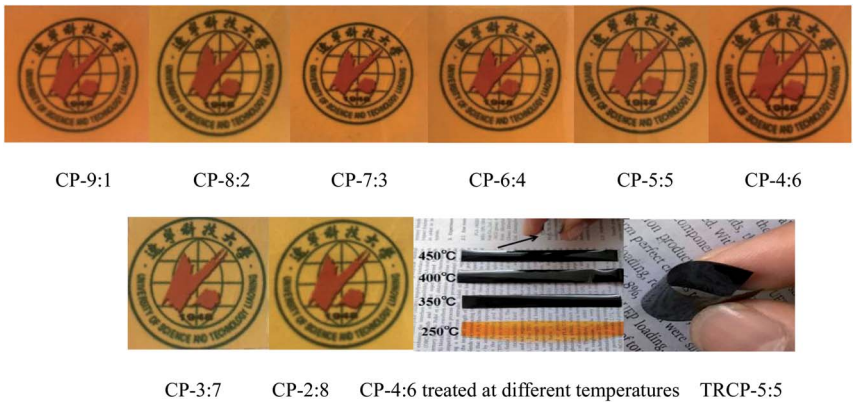

Fig. 1 Images of copolymer precursors and TR membranes.

1372 cm^{-1} is attributed to the stretching vibration of C–N bond in imide ring, and the peak of ether bond is located at 910 cm^{-1}. Furthermore, the characteristic peak of C–F bond in 6FDA appears at 1262 cm^{-1}. These characteristic peaks indicate that these precursors have mostly undergone the imidization reaction.

The stress–strain curves of copolymer precursor membranes are given in Fig. 3, and the corresponding mechanical properties data are listed in Table 1. According to the curves, these membranes show elastic deformation and fracture stages, but no obvious yield zone. The elongations at break of all samples are less than 4.0%, indicating the obvious rigidity characteristic of the macromolecular chain. Despite the presence of flexible ether bonds, the rigid and bulky fluorene groups effectively hinder the movement or rotation of molecular chains, and reduce the interaction between molecular chains, resulting in poor toughness. Moreover, the copolymerization is obviously affected by activity of diamines, so the molecular weight and its distribution of copolymers should be diverse, resulting in some irregular change of mechanical properties. Especially, when the molar ratio of BAHPPF to BAHPF was 1 : 9, the intact membrane was not obtained due to high rigidity, large volume structure and low reactivity of BAHPF. According to the experimental results, the tensile strength, Young's modulus and elongation at break of CP-5:5 and CP-4:6 were better than other samples, and the tensile strength reached 113.4 and 111.1 MPa, the elastic modulus attained 3.3 and 3.1 GPa, and the elongation at break achieved 4.0%, respectively. The results show that the appropriate copolymerization ratio of BAHPPF to BAHPF effectively improves the mechanical properties of precursor membrane materials to meet the further thermal rearrangement.

Dynamic mechanical analyzer DMA 8000 can not only accurately measure the glass transition temperature (T_g) of polymers, but also explore other thermal relaxation behaviors during the test. The Tan δ–T curves of precursor samples are shown in Fig. 4, which mainly include two or three obvious relaxation stages. The γ relaxation below 200 °C probably corresponds to some sub-glass relaxation related to local mobility due to the existence of ether linkage. The β relaxation below 300 °C is largely caused by further thermal imidization. The biggest α relaxation is ascribed to the transitions from glassy state to rubber state of the molecular chain. The temperature in this stage, corresponding to the peak of the loss factor (Tan δ), is commonly defined as the T_g. As shown in Table 1, the T_g values of these precursors are mainly concentrated at 337 to 389 °C, indicating that these precursors have excellent thermal properties. Although there are many flexible ether bonds in the polymer backbone, the bulky fluorenyl group

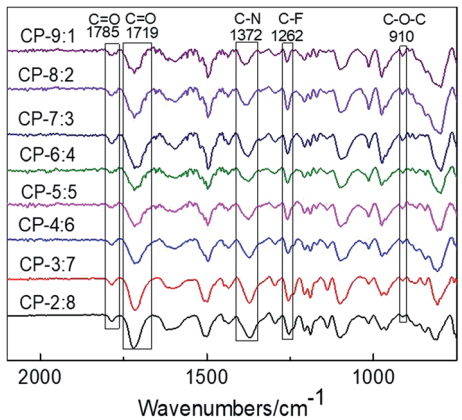

Fig. 2 Infrared spectra of copolymer precursors.

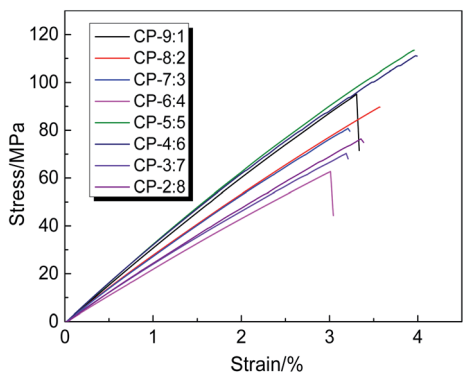

Fig. 3 Stress–strain curves of precursor membranes.

Table 1 Mechanical and thermal properties of precursor membranes

Samples	Average thickness (mm)	T_g[a] (°C)	T_{TR}[b] (°C)	Tensile strength (MPa)	Young's modulus (GPa)	Elongation at break (%)
CP-9:1	0.044	345	419	95.1 ± 3.0	2.9 ± 0.2	3.3 ± 0.2
CP-8:2	0.049	361	419	89.7 ± 4.0	2.8 ± 0.1	3.6 ± 0.1
CP-7:3	0.053	366	418	80.8 ± 2.0	2.7 ± 0.1	3.2 ± 0.1
CP-6:4	0.050	389	424	62.7 ± 4.0	2.2 ± 0.1	3.0 ± 0.3
CP-5:5	0.059	344	425	113.4 ± 2.0	3.3 ± 0.2	4.0 ± 0.1
CP-4:6	0.077	347	425	111.1 ± 3.0	3.1 ± 0.2	4.0 ± 0.1
CP-3:7	0.067	362	423	70.3 ± 3.0	2.4 ± 0.3	3.2 ± 0.2
CP-2:8	0.050	366	424	76.4 ± 4.0	2.4 ± 0.1	3.4 ± 0.1

[a] T_g: the glass transition temperature was estimated by Tan δ–T curves measured by DMA. [b] T_{TR}: the temperature at the maximum rate of thermally induced rearrangement was obtained by DTG–T curve.

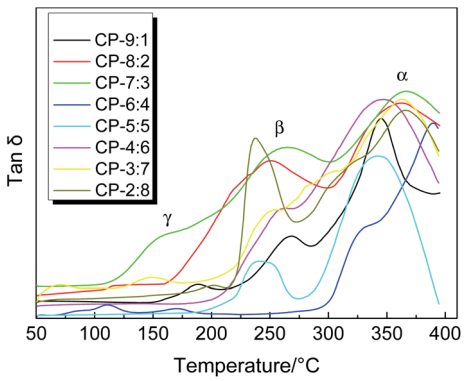

Fig. 4 Tan δ–T curve of copolymer precursor membranes.

provides larger steric hindrance for the movement and rotation of molecular chain and reduces the interaction between molecular chains, resulting in excellent thermal properties. In general, the copolymers with more flexible ether linkages, irregular arrangement and lower molecular weight possibly exhibit lower T_g values, such as CP-9:1, CP-5:5 and CP-6:4. Due to the relatively fast heating rate of 10 °C min^{-1} during the DMA testing, the obtained T_g values are higher, but the effect of molar ratio of diamines on the thermal properties is obviously displayed.

Thermogravimetric analysis was used to study the thermal stability and thermal rearrangement process of copolymer precursor samples. The TGA–T and DTG–T curves are shown in Fig. 5. It can be seen that the process of weight loss are roughly divided into three stages. The first slight mass loss between 250 °C and 370 °C is mainly caused by the volatilization of residual solvent and further imidization. The second prominent weight loss in the range of 370–480 °C is related to the release of CO_2 when the hydroxyl-containing copolymer precursor undergoes thermal rearrangement to form PBO. The thermal rearrangement temperature (T_{TR}) is defined as the temperature at the maximum conversion rate, which is listed in Table 1. The T_{TR} values of precursors are mainly around 420 °C, and the precursors with more ether bonds exhibit a relatively low T_{TR}, indicating that the rearrangement is closely related to the ability of segment movement.[10] Furthermore, we previously reported that the T_{TR} of HPEI (BAHPPF-6FDA) was 371 °C, while in this study the T_{TR} values of all copolymers were higher than that of HPEI, indicating that the introduction of BAHPF significantly increased the T_{TR} because of the rigid and bulky fluorene structure.[46] The third obvious weight loss appears when the temperature is higher than 480 °C, which is attributed to the

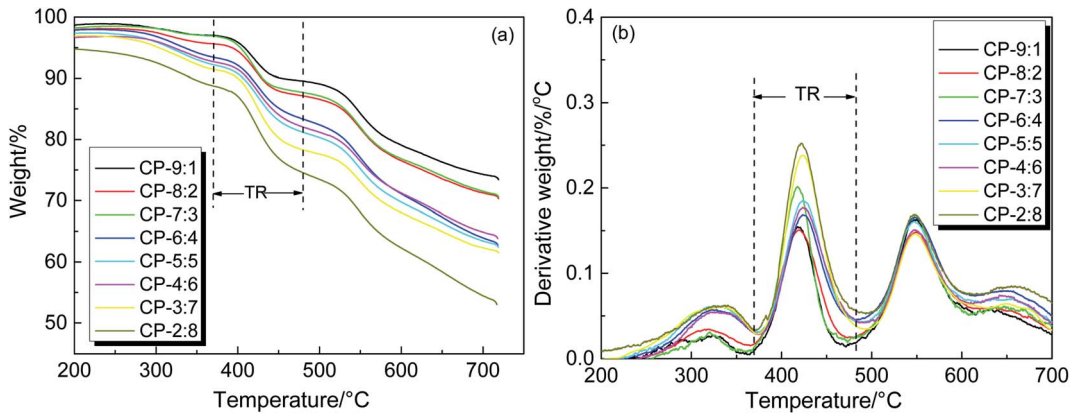

Fig. 5 TGA and DTG curves of copolymer precursor membranes (a) TGA; (b) DTG.

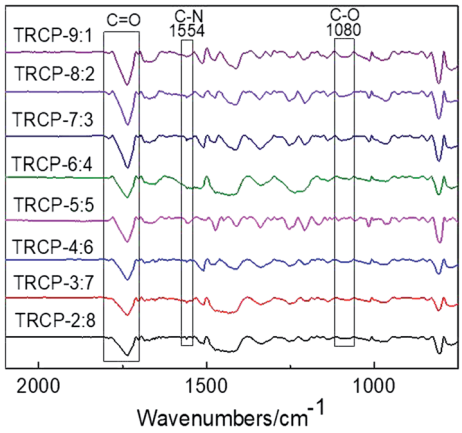

Fig. 6 Infrared spectra of TR membranes.

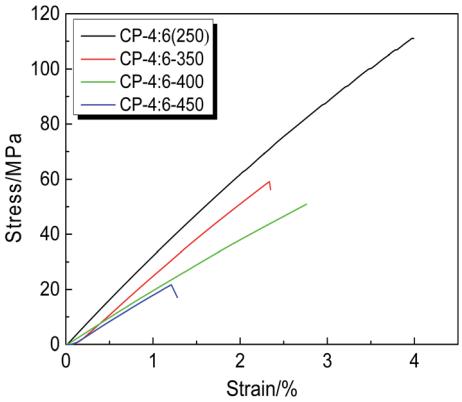

Fig. 7 Stress–strain curves of CP-4:6 membranes treated at different temperatures.

decomposition of polymer backbone. In this stage, the maximum mass loss rate of copolymers is mainly concentrated at about 550 °C, which indicates that these copolymers exhibit good thermal stabilities. According to the above analysis, the final thermal treatment temperature of the precursor samples was set at 450 °C for 1 hour, in order to complete most of the rearranged conversion and avoid the thermal decomposition.

3.2 Synthesis and characterization of TR copolymer membranes

The chemical structures of TR membranes obtained at 450 °C are characterized by FTIR and presented in Fig. 6. Compared with the copolymers without rearrangement, the asymmetric and symmetric stretching vibration absorption peaks corresponding to C=O bond at 1785 cm^{-1} and 1719 cm^{-1} are obviously weakened, and the characteristic absorption peaks of benzoxazole (N=C–O) appear at 1554 cm^{-1} and 1080 cm^{-1} respectively, indicating that the imide ring undergoes rearrangement reaction to form benzoxazole structures.

The mechanical properties of TR polymers are extremely important for their future industrial applications. In order to investigate the change of mechanical properties induced by thermal treatment, the CP-4:6 was selected and thermally treated at 350 °C, 400 °C and 450 °C for 1 hour, respectively. The stress–strain curves and corresponding mechanical properties are shown in Fig. 7 and Table 2, and the images of these membranes are given in Fig. 1. It is obvious that the color of the samples has changed from brown to black after thermal treatment, but these membranes still remain good flexibility. With the increase of thermal treatment temperature, the mechanical properties decreased sharply. Compared with the copolymer precursor membrane (250 °C), the tensile strength, Young's modulus and elongation at break of TR membrane (450 °C) decreased by 81%, 42% and 70%, respectively. Although the formation of benzoxazole structure was conducive to maintaining the rigidity of the main chain, a large number of micropores were produced due to the release of CO_2 during thermal rearrangement. In addition, a little decomposition of the backbone may occur, reducing the ability of the main chain to resist damage. It is reported that the mechanical properties of TR membranes were improved by introducing non-TR PI segments to meet the needs of testing and practical application, but the permeabilities of membrane materials had to be sacrificed.[38] In this study, CP-4:6–450 *i.e.* TRCP-4:6 still retained better mechanical properties by incorporating flexible ether linkages, and achieved higher gas permeabilities simultaneously. However, compared with spiroTR-PBO-BP-450 containing spiro ring structures, the mechanical data of TRCP-4:6-450 were lower.[40] The reason might be that the precursor of spiroTR-PBO-BP-450 was prepared by azeotropic imidization, leading to high molecular weight of 104 000 g mol^{-1} to enhance the mechanical properties of TR polymers.

Table 2 Mechanical properties of CP-4:6 treated at different temperatures

Samples	Tensile strength (MPa)	Young's modulus (GPa)	Elongation at break (%)	References
CP-4:6 (250)	111.1 ± 3.0	3.1 ± 0.2	4.0 ± 0.1	This work
CP-4:6-350	59.2 ± 4.0	2.1 ± 0.1	2.3 ± 0.2	This work
CP-4:6-400	50.9 ± 3.0	2.0 ± 0.2	2.7 ± 0.1	This work
CP-4:6-450	21.2 ± 2.0	1.8 ± 0.1	1.2 ± 0.3	This work
TPI-PBO-0.5-450	16 ± 3	2.27 ± 0.26	0.7 ± 0.1	38
TPI-PBO-0.75-450	13 ± 4	2.46 ± 0.40	0.6 ± 0.2	38
SpiroTR-PBO-BP-450	94.4	—	14.9	40

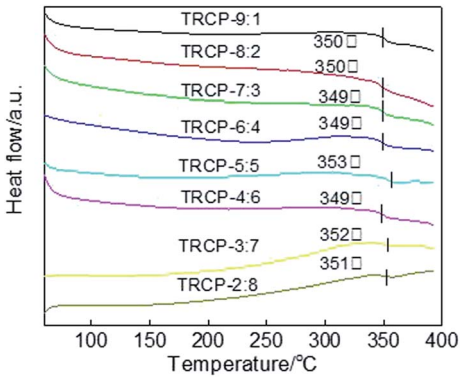

Fig. 8 DSC curves of TR copolymer samples.

The DSC curves of TR copolymers are shown in Fig. 8. Each DSC curve exhibits only one T_g, indicating that these polymers are random copolymers. Because the rigid fluorenyl and benzoxazole structure limit the movement of molecular segments, the T_g values of TR copolymers mainly center at about 350 °C. These membrane materials with excellent thermal properties could be suitable for high temperature environments.

XRD was used to characterize the microstructure of the precursors and TR membranes. As shown in Fig. 9, all precursors and TR copolymers exhibit no sharp diffraction peak, only a broad peak, which indicates that these polymers are primarily amorphous structures. The presence of rigid and bulky fluorenyl and $-CF_3$ groups effectively limits the regular packing of the macromolecular chain and increases the distance between molecular chains. According to the Bragg equation, the *d*-spacing values of copolymer precursors are mostly concentrated at 0.53 nm. After the thermal rearrangement, the amorphous characteristics are more obvious, and the *d*-spacing values of TR copolymers are significantly increased, which is ascribed to the formation of rigid polybenzoxazole backbone and the release of small molecular gas CO_2. By comparison, TRCP-4:6 showed the maximum *d*-spacing value of 0.60 nm, which could provide larger transmission channels for the small molecule gases.

The XPS analysis was utilized to study the change of chemical structure between precursors and TR copolymers. As shown in Fig. 10(a) and (b), the general XPS spectra give a valuable insight of CP-4:6 and TRCP-4:6 samples, indicating the presence of C, N, O and F elements. The fitting curves of O and N suggest that the benzoxazole structures have been formed from copolymer precursors containing hydroxyl groups. In Fig. 10(c) and (d), there are two fitting peaks at 533.5 eV and 532.0 eV, which are assigned to C–O of ether linkage and C═O in imide ring. Compared with Fig. 10(c), the proportion of fitting peak at 533.5 eV (C–O) in Fig. 10(d) obviously increased due to the partial conversion from C═O in imide ring to C–O of benzoxazole structure. Fig. 10(e) shows only one fitting peak at 400.4 eV, corresponding to –N< of imide ring, while there are two fitting peaks at 399.0 eV (C═N– of benzoxazole ring) and 400.4 eV (–N< of imide ring) in Fig. 10(f). Based on the area of two fitting peaks, the proportion of benzoxazole rings is about 76%, indicating that the thermal conversion was approximately completed by 76%.

3.3 Gas separation performance

Based on the same dianhydride 6FDA, the molar ratio of two diamines has affected the mechanical and thermal properties of copolymer membranes, which may influence the gas permeabilities of the resultant TR membranes. In order to evaluate the gas separation performance of TR copolymers, five kinds of high purity gases including H_2, N_2, O_2, CH_4 and CO_2 were used to test the gas permeation properties of these membrane materials. The gas permeabilities and ideal selectivities are summarized in Table 3.

As shown in Table 3, the gas permeabilities of TR membranes, except for TRCP-4:6, mainly follow the order: P (H_2) >P (CO_2) > P (O_2) >P (N_2) >P (CH_4), which is just opposite to the order of the dynamic diameter of gas molecules: H_2 (0.289 nm) < CO_2 (0.33 nm) < O_2 (0.346 nm) < N_2 (0.364 nm) < CH_4 (0.38 nm). Nevertheless, for the TRCP-4:6 membrane, the permeability of H_2 is less than that of CO_2, which is similar to the result of polymers of intrinsic microporosity (PIM) reported in the literature.[39] The TRCP-4:6 probably forms a large amount of

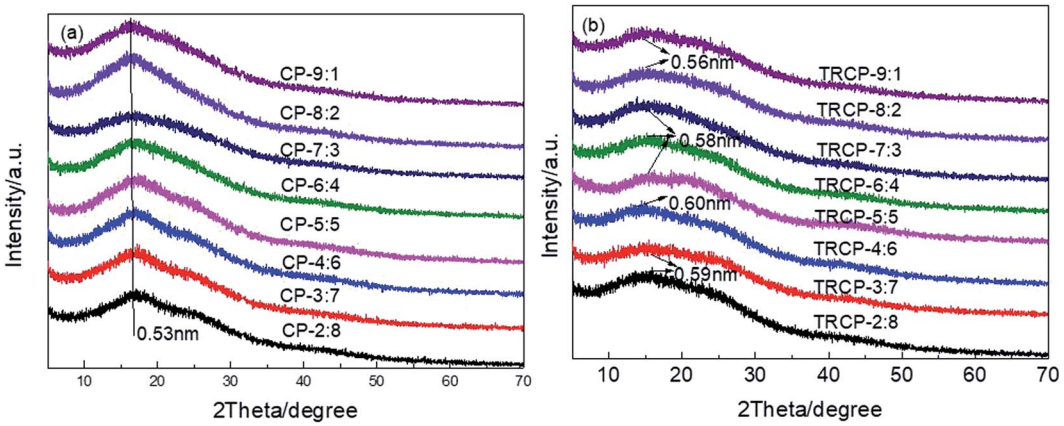

Fig. 9 XRD curves (a) copolymer precursors; (b) TR copolymers.

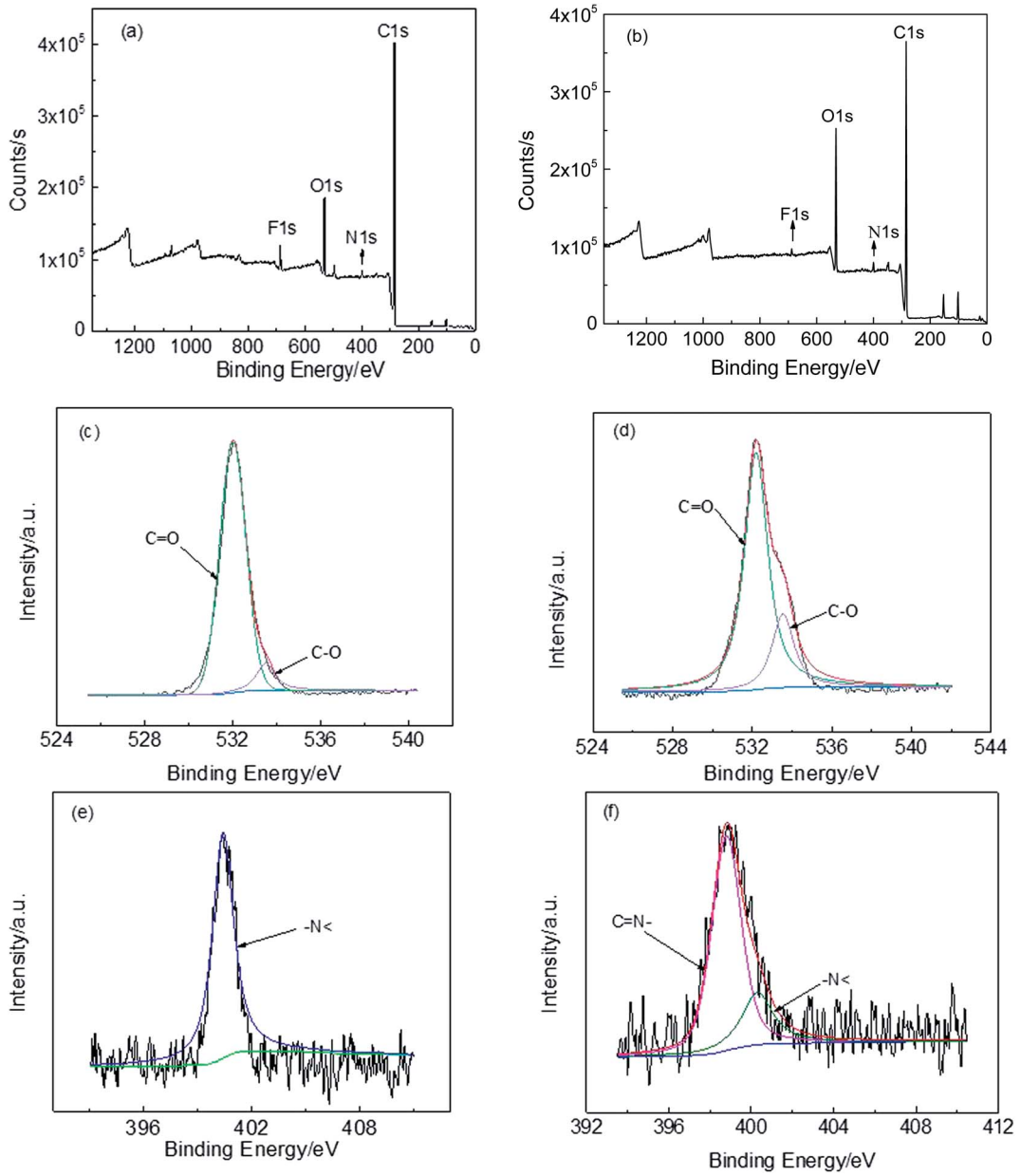

Fig. 10 XPS spectra (a) wide-scan spectrum of CP-4:6, (b) wide scan spectrum of TRCP-4:6, (c) O fitting curve of CP-4:6, (d) O fitting curve of TRCP-4:6, (e) N fitting curve of CP-4:6 and (f) N fitting curve of TRCP-4:6.

free volume, which is beneficial to diffusion of small molecules in the polymer. Generally, the gas permeabilities of TR membranes increased with the BAHPF content increasing. Especially, TRCP-4:6 and TRCP-3:7 exhibited better gas permeabilities than other TR copolymers, while the selectivity of CO_2/CH_4 was over 58, indicating high gas permeabilities coupled with high selectivities. It is interesting that the gas permeabilities and selectivities are improved at the same time, and there is no trade-off relationship. Besides, it was found that the TR copolymers with more flexible ether bonds showed relatively lower gas permeabilities, which was probably attributed to the close accumulation of molecular chains, reducing the channels for gas molecules to pass through the polymer. Among them, the H_2, CO_2, O_2, N_2 and CH_4 permeabilities of TRCP-4:6 membrane reached 244.4, 269.0, 46.8, 5.20 and 4.60 Barrers respectively, coupled with the O_2/N_2 of 9.00 and CO_2/CH_4 of 58.48. Compared with some reported TR polymers in Table 3, TRCP-4:6 exhibited excellent gas permeabilities and ideal selectivities, simultaneously. The results show that the excellent gas permeabilities coupled with ideal selectivities could be attained by effectively adjusting copolymerization ratio. The reasonable collocation of rigid structures and flexible linkages optimizes the shape of the "hourglass" to form effective gas permeation and separation channels. Additionally, the XRD results were largely consistent with the gas separation results. Therefore, these TR copolymers, especially TRCP-4:6, show

Table 3 Gas separation performance of TR membranes

	Permeabilities[a]/Barrer[b]					Ideal selectivities[c]	
Samples	H_2	CO_2	O_2	N_2	CH_4	O_2/N_2	CO_2/CH_4
TRCP-9:1	135.5	119.9	20.5	6.05	—	3.39	—
TRCP-8:2	143.1	124.8	22.9	5.29	—	4.33	—
TRCP-7:3	180.5	155.4	24.8	5.20	—	4.77	—
TRCP-6:4	189.9	163.0	30.0	8.40	3.62	3.57	45.03
TRCP-5:5	213.8	196.4	39.5	5.69	4.21	6.94	46.65
TRCP-4:6	244.4	269.0	46.8	5.20	4.60	9.00	58.48
TRCP-3:7	247.1	241.3	41.8	9.84	4.10	4.25	58.85
TRCP-2:8	214.0	201.3	34.4	7.14	4.15	4.82	48.51
TR-PEBO-450-1 (ref. 47)	95.3	41.4	10.0	1.89	1.45	5.3	28.6
TR-PBOI-c-420 (ref. 48)	—	61.9	14.3	3.2	1.48	4.47	41.8
TR-APAF-TP[49]	—	111	28.7	5.72	3.12	5.0	36
O-PIM-PBO-1 (ref. 39)	245	257	47	11	10	4.3	26
spiroTR-PBO-6F[50]	429	675	120	30	34	3.9	20
SPDA-SBF-PBO[51]	775	1280	225	61.6	84.8	3.7	15.1

[a] All permeation results were obtained at 30 °C and 0.01 MPa. [b] 1 Barrer = 10^{-10} $cm_{(STP)}^3$ cm cm^{-2} s^{-1} cm_{Hg}^{-1} = 3.35×10^{-16} mol m m^{-2} s^{-1} Pa^{-1}. [c] Permeability ratio of two gases.

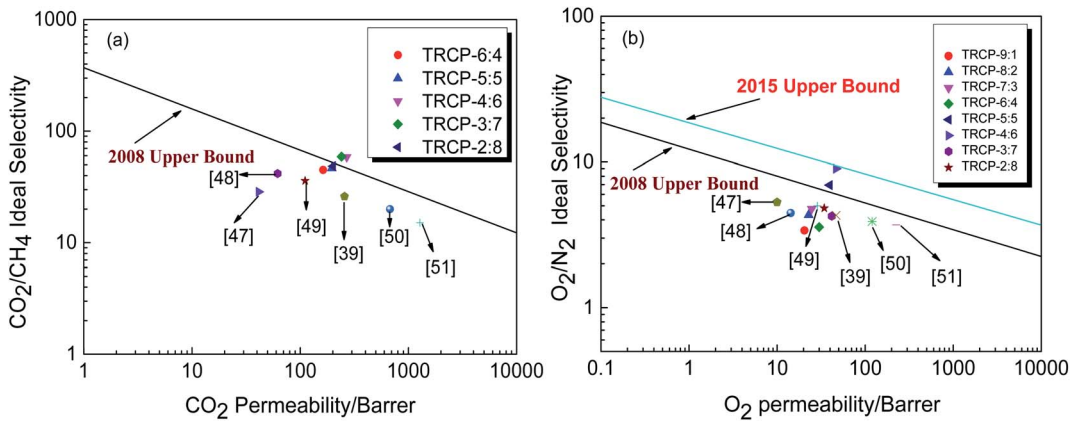

Fig. 11 Relationship between gas permeability and selectivity of TR membranes (a) CO_2 *vs.* CO_2/CH_4; (b) O_2 *vs.* O_2/N_2.

higher gas permeabilities and selectivities, as well as better mechanical and thermal properties, displaying excellent comprehensive performance.

In order to further evaluate the gas separation performance of membrane materials, Robeson summarized the hypothetical upper limit of the relationship between gas permeability and selectivity for valuable gas pairs, and proposed the 1991, 2008 and 2015 "upper limit".[9] The increase of the upper limit indicates that the separation efficiency of membrane materials has been improved significantly with the efforts of researchers and engineers, including the molecular structure design of new polymer materials and the effective development of mixed matrix membrane materials. As shown in Fig. 11(a), the five kinds of fluorene-based TR copolymer membranes exceed or approach the 2008 trade-off line for CO_2/CH_4 separation. Especially, TRCP-3:7 and TRCP-4:6 have exceeded the 2008 upper bound, showing high separation efficiency. According to Fig. 11(b), the separation performance of TRCP-4:6 for O_2/N_2 is very close to the 2015 upper bound, implying better gas separation behavior. Therefore, the proper copolymerization of BAHPF and BAHPPF not only improves the gas permeation flux, but also enhances the separation selectivities. These TR membranes are expected to be applied to the field of gas separation in the future.

4. Conclusions

A series of TR copolymer membranes were prepared by the copolymerization of 9,9-bis(3-amino-4-hydroxyphenoxyphenyl) fluorene (BAHPPF), 9,9-bis(3-amino-4-hydroxyphenyl)fluorene (BAHPF) and 2,2′-bis(3,4′-dicarboxyphenyl)hexafluoropropane dianhydride (6FDA), followed by thermal imidization and thermal rearrangement reactions. The copolymers as precursor showed excellent mechanical and thermal properties, especially CP-4:6 and CP-3:7. After thermal rearrangement at 450 °C, the TRCP-4:6 still remained better mechanical properties, including

tensile strength of 21.2 MPa, Young's modulus of 1.8 GPa and breaking elongation of 1.2%. In general, the gas permeabilities of resulting TR membranes increased with the increase of BAHPF content. Especially, the permeabilities of H_2, CO_2, O_2, N_2 and CH_4 for TRCP-4:6 reached 244.4, 269.0, 46.8, 5.20 and 4.60 Barrers respectively, and the CO_2/CH_4 selectivities of 58.48 and O_2/N_2 selectivities of 9.00 exceeded the 2008 upper bound. More importantly, by adjusting the molar ratio of diamines, the TR copolymers successfully attained better gas permeabilities, coupled with higher selectivities simultaneously, which broke away from the conventional trade-off rules. Therefore, the TR copolymer membranes exhibit outstanding mechanical, thermal and gas separation properties, which are expected to be applied in the field of gas separation in the future.

Conflicts of interest

There are no conflicts of interest to declare.

Acknowledgements

This work was financially supported by the National Natural Science Foundation of China (Grant number: 21878033), and University of Science and Technology Liaoning Talent Project Grants (Grant number: 601011507-17).

References

1 J. H. Lee, J. Lee, H. J. Jo, J. G. Seong, J. S. Kim, W. H. Lee, J. Moon, D. Lee, W. J. Oh, J. G. Yeo and Y. M. Lee, *J. Membr. Sci.*, 2017, **539**, 412–420.
2 Y. Liu, Z. Liu, A. Morisato, N. Bhuwania, D. Chinn and W. J. Koros, *J. Membr. Sci.*, 2020, **601**, 117910.
3 H. Borjigin, Q. Liu, W. Zhang, K. Gaines, J. S. Riffle, D. R. Paul, B. D. Freeman and J. E. McGrath, *Polymer*, 2015, **75**, 199–210.
4 H. Sanaeepur, A. E. Amooghin, S. Bandehali, A. Moghadassi and B. V. Bruggen, *Prog. Polym. Sci.*, 2019, **91**, 80–125.
5 Y. Xie, T. T. Wang, X. H. Liu, K. Zou and W. Q. Deng, *Nat. Commun.*, 2013, **4**, 1960–1966.
6 C. Zhang, P. Li and B. Cao, *J. Membr. Sci.*, 2017, **528**, 206–216.
7 L. M. Robeson, *J. Membr. Sci.*, 1991, **62**, 165–185.
8 L. M. Robeson, *J. Membr. Sci.*, 2008, **320**, 390–400.
9 R. Swaidan, B. Ghanem and I. Pinnau, *ACS Macro Lett.*, 2015, **4**, 947–951.
10 R. Guo, D. F. Sanders, Z. P. Smith, B. D. Freeman, D. R. Paul and J. E. McGrath, *J. Mater. Chem. A*, 2013, **1**, 6063–6072.
11 S. Kim, J. Hou, Y. Wang, R. Ou, G. P. Simon, J. G. Seong, Y. M. Lee and H. Wang, *J. Mater. Chem. A*, 2018, **6**, 7668–7674.
12 A. E. Amooghin, S. Mashhadikhan, H. Sanaeepur, A. Moghadassi, T. Matsuura and S. Ramakrishna, *Prog. Mater. Sci.*, 2018, **102**, 222–295.
13 Y. M. Xu, N. L. Le, J. Zuo and T. S. Chung, *J. Membr. Sci.*, 2016, **499**, 317–325.
14 N. Du, H. B. Park, M. M. Dal-Cin and M. D. Guiver, *Energy Environ. Sci.*, 2012, **5**, 7306–7322.
15 H. Wang, D. R. Paul and T.-S. Chung, *Polymer*, 2013, **54**, 2324–2334.
16 G. Tullos and L. Mathias, *Polymer*, 1999, **40**, 3463–3468.
17 G. L. Diego and L. Dmitri, *Polym. Bull.*, 2002, **48**, 261–269.
18 H. B. Park, S. H. Han, C. H. Jung, Y. M. Lee and A. J. Hill, *J. Membr. Sci.*, 2009, **359**, 11–24.
19 S. H. Han, N. Misdan, S. Kim, C. M. Doherty, A. J. Hill and Y. M. Lee, *Macromolecules*, 2010, **43**, 7657–7667.
20 C. Y. Soo, H. J. Jo, Y. M. Lee, J. R. Quay and M. K. Murphy, *J. Membr. Sci.*, 2013, **444**, 365–377.
21 C. A. Scholes, C. P. Ribeiro, S. E. Kentish and B. D. Freeman, *Sep. Purif. Technol.*, 2014, **124**, 134–140.
22 H. B. Park, C. H. Jung, Y. M. Lee, A. J. Hill, S. J. Pas, S. T. Mudie, E. Van Wagner, B. D. Freeman and D. J. Cookson, *Science*, 2007, **318**, 254–258.
23 S. Kim and Y. M. Lee, *Prog. Polym. Sci.*, 2015, **43**, 1–32.
24 Y. Jiang, F. T. Willmore, D. Sanders, Z. P. Smith, C. P. Ribeiro, C. M. Doherty, A. Thornton, A. J. Hill, B. D. Freeman and I. C. Sanchez, *Polymer*, 2011, **52**, 2244–2254.
25 A. K. Pate and N. K. Acharya, *Int. J. Hydrogen Energy*, 2020, **45**, 18685–18692.
26 K. A. Stevens, Z. P. Smith, K. L. Gleason, M. Galizia, D. R. Paul and B. D. Freeman, *J. Membr. Sci.*, 2017, **533**, 75–83.
27 M. Galizia, K. A. Stevens, D. R. Paul and B. D. Freeman, *J. Membr. Sci.*, 2017, **537**, 83–92.
28 A. Brunetti, M. Cersosimo, J. S. Kim, G. Dong, E. Fontananova, Y. M. Lee, E. Drioli and G. Barbieri, *Int. J. Greenh. Gas. Con.*, 2017, **61**, 16–26.
29 X. Jiang, X. Xiao, J. Dong, X. Xu, X. Zhao and Q. Zhang, *J. Membr. Sci.*, 2018, **564**, 605–616.
30 C. A. Scholes and B. D. Freeman, *J. Membr. Sci.*, 2018, **563**, 676–683.
31 W. Liu and W. Xie, *Ind. Eng. Chem. Res.*, 2013, **53**, 871–879.
32 M. Calle, H. J. Jo, C. M. Doherty, A. J. Hill and Y. M. Lee, *Macromolecules*, 2015, **48**, 2603–2613.
33 X. Hu, W. H. Lee, J. Zhao, J. S. Kim, Z. Wang, J. Yan, Y. Zhuang and Y. M. Lee, *J. Membr. Sci.*, 2020, **604**, 118053.
34 C. Aguilar-Lugo, C. Álvarez, Y. M. Lee, J. G. de la Campa and Á. E. Lozano, *Macromolecules*, 2018, **51**, 1605–1619.
35 J. I. Choi, C. H. Jung, S. H. Han, H. B. Park and Y. M. Lee, *J. Membr. Sci.*, 2009, **349**, 358–368.
36 X. Ma, R. Swaidan, B. Teng, H. Tan, O. Salinas, E. Litwiller, Y. Han and I. Pinnau, *Carbon*, 2013, **62**, 88–96.
37 S. M. Meckler, J. E. Bachman, B. P. Robertson, C. Zhu, J. R. Long and B. A. Helms, *Angew. Chem., Int. Ed.*, 2018, **57**, 4912–4916.
38 S. Luo, Q. Zhang, T. K. Bear, T. E. Curtis, R. K. Curtis, C. M. Doherty, A. J. Hill and R. Guo, *J. Membr. Sci.*, 2018, **551**, 305–314.
39 H. Shamsipur, B. A. Dawood, P. M. Budd, P. Bernardo, G. Clarizia and J. C. Jansen, *Macromolecules*, 2014, **47**, 5595–5606.
40 Q. Liu, D. R. Paul and B. D. Freeman, *Polymer*, 2016, **82**, 378–391.

41 A. Tena, S. Rangou, S. Shishatskiy, V. Filiz and V. Abetz, *Sci. Adv.*, 2016, **2**, e1501859.
42 S. Kim, K. T. Woo, J. M. Lee, J. R. Quay, M. K. Murphy and Y. M. Lee, *J. Membr. Sci.*, 2014, **453**, 556–565.
43 F. Alghunaimi, B. Ghanem, Y. Wang, O. Salinas, N. Alaslai and I. Pinnau, *Polymer*, 2017, **121**, 9–16.
44 Y. F. Yeong, H. Wang, K. P. Pramoda and T. S. Chung, *J. Membr. Sci.*, 2012, **397**, 51–65.
45 Y. Lu, J. Hao, L. Li, J. Song, G. Xiao, H. Zhao, Z. Hu and T. Wang, *React. Funct. Polym.*, 2017, **119**, 134–144.
46 Y. Lu, J. Zhang, G. Xiao, L. Li, M. Hou, J. Hu and T. Wang, *RSC Adv.*, 2020, **10**, 17461–17472.
47 M. Calle and Y. M. Lee, *Macromolecules*, 2011, **44**, 1156–1165.
48 F. Gan, J. Dong, X. Xu, M. Li, X. Zhao and Q. Zhang, *Polymer*, 2019, **185**, 121945.
49 B. Díez, P. Cuadrado, Á. Marcos-Fernández, J. G. de la Campa, A. T. Tena, P. Prádanos, L. Palacio, Y. M. Lee, C. Alvarez, Á. E. Lozano and A. Hernández, *React. Funct. Polym.*, 2018, **127**, 38–47.
50 S. Li, H. J. Jo, S. H. Han, C. H. Park, S. Kim, P. M. Budd and Y. M. Lee, *J. Membr. Sci.*, 2013, **434**, 137–147.
51 X. Ma, O. Salinas, E. Litwiller and I. Pinnau, *Polym. Chem.*, 2014, **5**, 6914–6922.